Published in final edited form as:
Neuron. 2013 June 19; 78(6): . doi:10.1016/j.neuron.2013.04.025.

Dendritic Peptide Release Mediates Interpopulation Crosstalk between Neurosecretory and Preautonomic Networks

Sook Jin Son[1], **Jessica A. Filosa**[1], **Evgeniy S. Potapenko**[1], **Vinicia C. Biancardi**[1], **Hong Zheng**[2], **Kaushik P. Patel**[2], **Vicky A. Tobin**[3], **Mike Ludwig**[3], and **Javier E. Stern**[1,*]

[1]Department of Physiology, Georgia Regents University, Augusta, GA 30912, USA

[2]Department of Cellular and Integrative Physiology, University of Nebraska Medical Center, Omaha, NE 68198, USA

[3]Centre for Integrative Physiology, University of Edinburgh, Edinburgh EH8 9XD, UK

SUMMARY

Although communication between neurons is considered a function of the synapse, neurons also release neurotransmitter from their dendrites. We found that dendritic transmitter release coordinates activity across distinct neuronal populations to generate integrative homeostatic responses. We show that activity-dependent vasopressin release from hypothalamic neuroendocrine neurons in the paraventricular nucleus stimulates neighboring (~100 μm soma-to-soma) presympathetic neurons, resulting in a sympathoexcitatory population response. This interpopulation crosstalk was engaged by an NMDA-mediated increase in dendritic Ca^{2+}, influenced by vasopressin's ability to diffuse in the extracellular space, and involved activation of CAN channels at the target neurons. Furthermore, we demonstrate that this interpopulation crosstalk plays a pivotal role in the generation of a systemic, polymodal neurohumoral response to a hyperosmotic challenge. Because dendritic release is emerging as a widespread process, our results suggest that a similar mechanism could mediate interpopulation crosstalk in other brain systems, particularly those involved in generating complex behaviors.

INTRODUCTION

Information processing in the CNS involves a wide array of spatiotemporal scales, ranging from temporally fast and spatially precise (critical for coherent spike timing between two neurons; Galarreta and Hestrin, 2001), to temporally slow and spatially diffuse, a modality best suited for the coordination of activity within or across entire neuronal populations (Fuxe et al., 2007; Leng and Ludwig, 2008). Despite the importance of the latter in the generation of complex behaviors (Ludwig and Leng, 2006), the precise signaling mechanisms underlying interpopulation crosstalk in the brain remain largely unknown.

Neuropeptides are increasingly recognized as unique signals involved in information processing in the brain (Leng and Ludwig, 2008; Salio et al., 2006). They are abundantly found in dendrites (Guan et al., 2005; Pow and Morris, 1989), their release is generally not confined to or targeted at synaptic/postsynaptic sites, and given their relatively long half-lives (Mens et al., 1983), they can diffuse in the extracellular space (ECS) to act on distant

*Correspondence: jstern@gru.eduhttp://dx.doi.org/10.1016/j.neuron.2013.04.025.

SUPPLEMENTAL INFORMATION Supplemental Information includes Supplemental Experimental Procedures and seven figures and can be found with this article online at http://dx.doi.org/10.1016/j.neuron.2013.04.025.

targets. Thus, unlike classical fast-acting neurotransmitters, neuropeptide signaling lacks temporal and spatial precision, making it ideally suited to mediate communication between populations of neurons (Fuxe et al., 2007; Landgraf and Neumann, 2004; Ludwig and Leng, 2006).

Neuropeptides are widely used as signaling molecules in the hypothalamus, particularly within the supraoptic and paraventricular nuclei (SON and PVN, respectively). These centers are critically involved in the generation of complex polymodal homeostatic responses, consisting of orchestrated activities of autonomic and neuroendocrine networks (Buijs and Van Eden, 2000; Swanson and Sawchenko, 1980). During disturbances of fluid/electrolyte homeostasis, activation of magnocellular neurosecretory (MNNs) and presympathetic neurons in the PVN results in the concerted systemic release of the hormone vasopressin (VP), along with an increase in renal sympathetic outflow, respectively, acting together to restore fluid/electrolyte balance (Bourque, 2008; Toney and Stocker, 2010). Importantly, an imbalanced interaction among these systems results in maladaptive responses characteristic of disease conditions, including stress and hypertension (Ely, 1995; Esler et al., 1995). Thus, generation of homeostatic responses by the PVN represents an ideal paradigm to study interpopulation signaling mechanisms within the brain, both under physiological and pathological conditions.

In addition to playing key roles in the processing and integration of synaptic inputs, dendrites are recognized to be major sources of brain neuropeptides (Guan et al., 2005; Pow and Morris, 1989), MNNs being one of the best-studied prototypes of dendritic peptide release (Ludwig and Leng, 2006). Besides releasing their peptide content from neurohypophyseal axonal terminals into the circulation, MNNs also release VP and oxytocin (OT) locally from their dendrites, serving as a powerful autocrine signal by which they autoregulate their activity (Gouzènes et al., 1998; Ludwig and Leng, 1997). However, whether dendritically released peptides from MNNs can act beyond their own secreting population, to mediate interpopulation crosstalk, has not yet being explored. Using the magnocellular neurosecretory system as a unique model system, we tested the hypothesis that dendritic peptide release constitutes a powerful interpopulation signaling modality in the brain. More specifically, we assessed whether dendritically released VP mediates crosstalk between neurosecretory and presympathetic hypothalamic neurons in the context of homeostatic neurohumoral responses to an osmotic challenge.

Using a combination of in vitro approaches in acute hypothalamic slices, including patch-clamp electrophysiology, confocal imaging, and laser photolysis of caged molecules, we demonstrate that dendritically released VP from a single stimulated neurosecretory neuron evoked a direct excitatory response in presympathetic neurons located ~100 μm away. Moreover, we found that activity-dependent dendritic VP release from the whole population of neurosecretory neurons translated into a diffusible pool of peptide that tonically stimulated presympathetic neuronal activity. Finally, using an in vivo homeostatic challenge, we show that dendritic VP release is critical for the recruitment of presympathetic neurons, resulting in an optimal sympathoexcitatory outflow during a homeostatic challenge that requires an orchestrated neurosecretory and sympathetic response.

RESULTS

Intimate Dendro-Somatic and Dendro-Dendritic Interrelationships between Presympathetic and Magnocellular Neurosecretory PVN Neurons

It is well documented that neurosecretory and presympathetic neuronal somata in the PVN are anatomically compartmentalized within specific subnuclei (Swanson and Kuypers, 1980; Swanson and Sawchenko, 1980). Using a combination of retrograde tract tracing and

immunohistochemistry to identify presympathetic PVN neurons that innervate the rostroventrolateral medulla (RVLM; PVN-RVLM neurons) and VP MNNs, respectively, we verified this early observation (Figure 1A). However, a more detailed analysis revealed that thick and varicose dendritic processes from VP MNNs extended beyond their own neuronal compartment, coming in close proximity to somatodendritic elements of presympathetic neurons in the ventromedial, dorsal cap, and posterior parvocellular subnuclei (Swanson and Kuypers, 1980) (Figures 1B–1G). The identity of these processes as dendrites was confirmed by microtubule-associated protein 2 (MAP2) immunoreactivity (Figure 1I) and by being abutted by numerous dopamine β hydroxylase (DBH)-immunoreactive presynaptic boutons (Figure 1J). Conversely, VP axons ran laterally out of the PVN boundaries, then turned ventrally and caudally toward the median eminence (Figure 1H) (Swanson and Kuypers, 1980). These studies support thus a distinctive anatomical microenvironment that would enable dendro-dendritic/somatic communication from neurosecretory to presympathetic neurons, possibly via dendritically released VP.

Activation of V1a Receptors in Presympathetic PVN Neurons Increases Their Firing Activity via a Ca^{2+}-Dependent Activation of a CAN Channel

To determine if presympathetic neurons sense dendritically released VP from MNNs, we first assessed for the expression of V1a receptors (the most common type of VP receptor found in the brain; Zingg, 1996) in retrogradely labeled PVN-RVLM neurons. As shown in Figures 2A–2D, we found a dense V1a receptor immunoreactivity in somatodendritic regions of presympathetic neurons. Similar results were found with an alternative V1a antibody (Figure S1 available online), recently shown to label V1a receptors in olfactory bulb neurons (Tobin et al., 2010). The resolution of the light microscopic approach, however, does not readily distinguish V1a clusters located near the surface membrane of PVN-RVLM neurons from ones potentially located at presynaptic terminals. Further supporting the expression of V1a receptors by PVN-RVLM neurons, however, we report expression of V1a receptor mRNA in this neuronal population (Figure 2E).

Focal application of VP onto presympathetic PVN neurons resulted in direct membrane depolarization and increased firing discharge ($n = 16$, $p < 0.001$; Figures 2F–2I). VP effects were almost completely blocked by a selective V1a receptor antagonist (β-mercapto-β,β-cyclopentamethylenepropionyl^1, [O-me-Tyr^2, Arg^8]-VP, 1 μM; $p < 0.01$, $n = 8$; Figure 2H) but persisted in the presence of the ionotropic glutamate and $GABA_A$ receptor antagonists kynurenate (1 mM) and bicuculline (20 μM) (basal, 0.30 ± 0.13 Hz; VP, 2.75 ± 0.53 Hz; $p < 0.01$, $n = 6$) or in the presence of a low Ca^{2+} synaptic block media (basal, 0.58 ± 0.38 Hz; VP, 3.85 ± 0.38 Hz; $p < 0.02$).

The VP-mediated increase in firing activity in presympathetic neurons was preceded (3.1 ± 0.8 s) by an increase in $[Ca^{2+}]_I$ ($p < 0.01$, $n = 8$; Figures 3A–3C) and was abolished by chelation of intracellular Ca^{2+} with BAPTA (10 mM) ($n = 8$; Figure 3D). In voltage-clamp mode, VP evoked an outwardly rectifying current with an apparent reversal potential of ~ −15 mV (Figure 3E). Taken together, these results support the involvement of a Ca^{2+}-activated nonselective cation current (CAN) (Petersen, 2002). We found PVN-RVLM neurons to express dense immunoreactivity (Figures S2A–S2D) and mRNA (Figure S2E) for TRPM4 channels, a major CAN channel member of the transient receptor potential (TRP) family (Ullrich et al., 2005), and previously reported in the hypothalamus (Ghamari-Langroudi and Bourque, 2002; Teruyama and Armstrong, 2007; Teruyama et al., 2011). We also found that VP excitatory effects on PVN-RVLM neurons were blocked by flufenamic acid (FFA; 200 μM) ($n = 9$; Figure S2F), a relatively specific blocker of TRPM4/TRPM5 channels (Ullrich et al., 2005). In the presence of FFA, PVN-RVLM neurons were still capable of displaying a burst of action potentials in response to a puff of 20 μM NMDA ($n = 3$; data not shown), indicating that FFA effects were not due to nonspecific effects on overall

neuronal function or due to changes in PVN-RVLM responsiveness to NMDA. Further studies, however, are needed to precisely identify the molecular identity of the CAN channel underlying VP actions in presympathetic neurons.

Dendritic Release of VP Mediates Cell-Cell Communication between Neighboring Neurosecretory and Presympathetic Neurons

To directly probe for a crosstalk between MNNs and presympathetic neurons, we developed an approach using transgenic EGFP-VP rats (Ueta et al., 2005) that received an injection of a fluorescent retrograde tracer in the RVLM (Figure S3). Our approach consisted of selectively activating individual VP neurons using laser photolysis of caged NMDA while simultaneously monitoring the electrical activity of neighboring presympathetic neurons in acute hypothalamic slices. To validate this approach, we show that laser photolysis of caged NMDA onto restricted somatodendritic regions of patched EGFP-VP neurosecretory neurons induced reproducible inward currents along with a concurrent high-frequency burst of action potentials (Figure 4A), previously shown to efficiently evoke dendritic release of peptides from MNNs in brain slices (Kombian et al., 1997). Moreover, photolysis of caged NMDA in the somata of Fluo-5F-loaded EGFP-VP neurons increased $[Ca^{2+}]_i$ levels, which rapidly propagated into dendritic compartments (Figure S4).

To test the hypothesis that dendritic VP release acts as a crosstalk signal between neurosecretory and presympathetic neurons, we then obtained patch recordings from PVN-RVLM neurons and assessed their responses to photolysis of caged NMDA in neighboring EGFP-VP neurons. On average, three different EGFP-VP neurons were photoactivated per patched PVN-RVLM neuron. The mean distance between the somata of presympathetic and the photoactivated VP neurons was 111.6 ± 7.9 μm. Photolysis of caged NMDA at the somata of individual EGFP-VP neurons consistently evoked an excitatory response in neighboring PVN-RVLM neurons, characterized by a burst of activity, which was underlain by a membrane depolarization (n = 38 EGFP-VP neurons/11 PVN-RVLM neurons, $p < 0.001$; Figure 4B). Responses in presympathetic neurons occurred with a mean latency of 3.5 ± 1.0 s following photolysis in neighboring EGFP-VP neurons. In a few cases (n = 4), stimulation of an EGFP-VP neuron failed to evoke a response in PVN-RVLM neurons, which were, however, responsive to other EGFP-VP neurons in the same preparation.

Direct photolysis of caged NMDA onto the recorded neurons (EGFP-VP or presympathetic) resulted in an almost instantaneous effect ($p < 0.05$, n = 11; Figure 4). Importantly, presympathetic responses to photoactivation of EGFP-VP neurons were almost completely blocked following bath application of the V1a receptor antagonist Figure 4C). No relationship between the uncaging distance and magnitude or delay of the evoked response was observed.

Although action potentials are necessary for axonal VP release, dendritic release can occur in a Ca^{2+}-dependent but action potential-independent manner (Ludwig et al., 2002). Thus, to rule out a potential, but unlikely, contribution of VP released from an axon collateral within the PVN (Hatton et al., 1985; Ludwig, 1998), experiments were repeated in the presence of 1 μM tetrodotoxin (TTX). Under these conditions, photolysis of NMDA onto EGFP-VP neurons still evoked a membrane depolarization in neighboring PVN-RVLM neurons (n = 18), effects that were blocked by the V1a receptor antagonist ($p < 0.01$, n = 14; Figure 5). Conversely, following activation of EGFP-VP neurons, presympathetic responses were prevented by a 0 Ca^{2+}/3 mM EGTA aCSF (Δ 1.2 ± 0.2 mV, n = 10, $p > 0.3$), without altering PVN-RVLM responses to direct uncaging of NMDA (Δ 5.5 ± 0.5 mV, $p < 0.05$, n = 4). These results support that Ca^{2+}-dependent dendritic release of VP (Ludwig et al., 2002) stimulates the activity of neighboring presympathetic PVN neurons via activation of V1a receptors.

To rule out the possibility that PVN-RVLM neuronal responses were due to diffusion of caged NMDA beyond the photoactivated region in the EGFP-VP neurons, a subset of recorded PVN-RVLM neurons was dialyzed with the NMDAR blocker MK-801 (1 mM). Although intracellular MK801 significantly blocked the effect of direct photolysis of caged NMDA onto the recorded neurons (Δ 1.3 ± 0.9 mV; $p > 0.2$, $n = 4$), photolysis onto EGFP-VP neurons still evoked a depolarizing response from the same PVN-RVLM neurons (Δ 5.2 ± 1.4 mV; $p < 0.05$, $n = 4$) (Figure S5). Additional controls included laser stimulation without the presence of caged NMDA and bath application of caged NMDA alone, both of which failed to evoke neuronal responses (data not shown). Finally, NMDA uncaging onto EGFP-VP neurons ($n = 33$) failed to evoke changes in $[Ca^{2+}]_I$ in the vast majority of Rhod-2-loaded astrocytes (~87%). In the few responsive astrocytes, increases in $[Ca^{2+}]_I$ occurred with a long delay (>40 s) (Figure S6).

To further prove the neurosecretory-presympathetic neuronal crosstalk, we performed dual-patch recordings from identified EGFP-VP and PVN-RVLM neurons. In 13 out of 15 pairs tested, we found that evoked burst firing in VP neurons resulted in a significant membrane depolarization ($p < 0.001$; $n = 13$) and increase in firing discharge ($p < 0.02$; $n = 13$) in the neighboring presympathetic neurons (Figures 6B and 6F). These effects were largely blocked following bath application of the V1a antagonist ($n = 7$) or in pairs in which EGFP-VP neurons were dialyzed with BAPTA ($n = 5$) (Figures 6C and 6F). No responses were observed in the remaining two pairs. We found that the latency for the evoked PVN-RVLM depolarization was significantly longer when a prominent afterhyperpolarizing potential (AHP) following the evoked bursts of action potentials was observed in the paired EGFP-VP neuron ($n = 9$; Figure 6B1), compared to neurons in which AHPs were absent ($n = 6$; Figure 6B2), or those in which a depolarizing afterpotential (DAP) was observed instead ($n = 3$; Figure 6D) ($p < 0.001$; Figure 6E). Moreover, a significant correlation between the EGFP-VP AHP duration and the PVN-RVLM latency was found (Pearson $r = 0.89$; $p < 0.0001$). The mean latency in paired recordings in which AHPs in EGFP-VP neurons were absent was similar to that observed following photolysis of caged NMDA ($p > 0.3$; see above), in which AHPs were not observed. In contrast to the effect on latency, the magnitude of the PVN-RVLM response was independent of the presence or duration of an AHP in the stimulated EGFP-VP neurons (data not shown).

Finally, to determine whether astrocytes participate as intermediaries in the neurosecretory-presympathetic crosstalk, experiments were repeated following functional ablation of astrocytes with the selective gliotoxin L-aminoadipic acid (L-AAA; 250 μM, 30–60 min) (McBean, 1994; Xu et al., 2008). Under this condition, stimulation of EGFP-VP neurons still efficiently evoked an excitatory response in PVN-RVLM neurons ($p < 0.001$, $n = 5$; (Figures 6D and 6F). In a few cases ($n = 4$) in which both neurons were intracellularly labeled with fluorescent dyes, segments of dendrites from the paired neurons were found in close proximity (12.5 ± 3.1 μm) (Figures 6G1–6G3).

An Activity-Dependent Diffusible VP Pool Tonically Stimulates Presympathetic Neuronal Activity

Our results demonstrate that evoked dendritic peptide release from an individual VP neuron can diffuse locally to affect the activity of a neighboring presympathetic neuron. We then tested whether the basal average activity of the neurosecretory VP population as a whole was sufficient to generate a tonic-diffusing peptide pool, to continuously modulate presympathetic neuronal activity. Blockade of V1a receptors per se resulted in membrane hyperpolarization and inhibition of firing activity in presympathetic neurons ($p < 0.001$ and $p < 0.01$, respectively, $n = 14$; Figures 7A and 7B), unveiling the presence of a diffusible, tonic pool of VP. Conversely, the firing activity of EGFP-VP neurons was not affected (baseline, 2.2 ± 0.6 Hz; V1a antagonist, 2.2 ± 0.7 Hz; $n = 5$). To test whether the strength of

the diffusible pool was dependent on the degree of activity of the VP population, we performed manipulations that either increased or decreased VP neuronal activity. The VP tone was enhanced by increasing extracellular K^+ concentration (8.0 mM K^+), as indicated by a more pronounced effect of the V1a antagonist in this condition, compared to normal K^+ ACSF ($p < 0.01$; Figure 7D). Conversely, in the presence of the κ opioid receptor agonist U-50488 (1 μM), known to strongly inhibit VP neuronal activity ($p < 0.01$; Figure S7A; see also Brown et al., 1998), the V1a antagonist effect on presympathetic neuronal activity was significantly blunted ($p < 0.05$ versus control; Figures 7C and 7D). In the presence of the V1a antagonist, however, U-50488 failed to affect the firing activity of presympathetic neurons ($p > 0.6$, $n = 4$; Figure S7B), arguing against a direct effect of U50488 on the latter. No correlation between basal PVN-RVLM firing activity and the magnitude of the V1a antagonist effect was found in any of these different conditions (Pearson $r = -0.02$; $p > 0.5$). Dialysis of BAPTA into the recorded PVN-RVLM neurons prevented the effects of the V1a antagonist (baseline, 0.7 ± 0.1 Hz; V1a antagonist, 0.6 ± 0.1 Hz; $p > 0.3$, $n = 6$).

A diffusible signal in the ECS could be influenced both by its half-life and the ECS tortuosity. Blockade of tissue aminopeptidase activity (amastatin 10 μM) increased the firing activity of presympathetic neurons ($p < 0.01$, $n = 8$; Figure 7E). The amastatin effect was not only blocked but also actually turned into an inhibitory effect in the presence of the V1a receptor blocker ($p < 0.01$ versus amastatin control, $n = 7$; Figure 7E). These results indicate that aminopeptidase blockade increased not only the availability and excitatory actions of endogenous VP but also of an unknown inhibitory signal, which was only unmasked when the VP excitatory effect was blocked. The identity of this inhibitory peptide signal was not further investigated in this study.

Reducing the coefficient of diffusion in the ECS with 5% dextran (40 kDa) (Min et al., 1998; Piet et al., 2004) also blocked the V1a antagonist effect on presympathetic firing discharge (−6.5% ± 8.8%; $p > 0.6$, $n = 4$). Taken together, these results indicate that tonically released VP within the PVN serves as a neurosecretory population signal, which acting in a diffusible manner, increased the activity of the presympathetic PVN neuronal population.

Dendritic Release of VP within the PVN Contributes to the Recruitment of Sympathetic Neurons during an Osmotic Challenge

We finally assessed whether dendritic release of VP serves as an interpopulation signal by which the integrated sympathoexcitatory output from the entire presympathetic neuronal population was modulated. To this end, we performed in vivo studies to directly monitor sympathoexcitatory outflow from the PVN. We found that direct microinjection of VP (8–32 pmol) onto the PVN elicited a dose-dependent sympathoexcitatory response, reflected by an increase in renal sympathetic nerve activity (RSNA; $p < 0.02$, $n = 9$; Figures 8A and 8B). These results indicate that the VP excitatory effect observed on presympathetic neurons in vitro translated into a systemic, population sympathoexcitatory response.

It is well documented that a central osmotic challenge results in a robust PVN homeostatic response that involves an orchestrated activation of VP MNNs and presympathetic neurons, leading to increased plasma VP levels along with a concomitant increase in sympathetic outflow, respectively (Bourque, 2008; Toney and Stocker, 2010). Thus, we used this paradigm to assess the functional relevance of the neurosecretory-presympathetic crosstalk in the context of a homeostatic challenge. Intracarotid infusions of graded concentrations of NaCl (0.3, 0.9, and 2.1 Osm/l) induced a significant and dose-dependent increase in RSNA ($p < 0.0001$, $n = 7$; Figures 8C and 8D). This osmotically driven sympathoexcitatory response was significantly attenuated (~50%) by a previous bilateral microinjection of the V1a antagonist within the PVN (2 nmol in 100 nl; $p < 0.001$ versus control; Figures 8C and

8D). As shown in Figure 8E, the intracarotid osmotic stimulation evoked a significant increase in VP release within the SON ($p < 0.001$, one-way ANOVA repeated measures; $n = 7$). These results indicate that osmotically driven dendritic VP release participates in the recruitment of presympathetic neurons during a homeostatic challenge requiring an orchestrated neurosecretory and sympathetic response.

DISCUSSION

The two modalities by which the PVN commands the generation of complex homeostatic responses are represented in distinct neuronal populations, including neurosecretory neurons projecting to the median eminence or the posterior pituitary, and presympathetic neurons innervating the spinal cord and/or brainstem nuclei, including the RVLM (Swanson and Sawchenko, 1980). Given its diverse, though well-characterized anatomical and functional organization, the PVN stands as an ideal brain region to study interpopulation signaling modalities in the brain. Despite its highly integrative function, it is well documented that neurosecretory and presympathetic PVN neuronal populations are anatomically compartmentalized, displaying a minimal or complete lack of hardwired interconnections (Hatton et al., 1985; Swanson and Kuypers, 1980; Swanson et al., 1980). This has led to the notion that polymodal homeostatic control by the PVN involves parallel processing of neuroendocrine and autonomic information. In this study, we challenged this prevailing idea by testing the hypothesis that dendritic release of peptides serves as an interpopulation signal mediating crosstalk between neurosecretory and presympathetic PVN neuronal populations. Along with nigrostriatal dopaminergic neurons (Cheramy et al., 1981), hypothalamic MNNs are one of the best-characterized prototypes of dendritic neurotransmitter release (Ludwig and Leng, 2006). Dendritic release of VP and OT from MNNs acts as powerful feedback signals by which MNNs autoregulate their own activity, to optimize systemic hormone release in response to physiologically relevant challenges (Kombian et al., 1997; Ludwig and Leng, 1997). Results from the present study demonstrate that in addition to its autocrine actions, VP acts as a diffusible signal to bridge information across neurosecretory and presympathetic neuronal populations. This crosstalk involves Ca^{2+}-dependent dendritic release of VP, diffusion in the ECS, and activation of V1a VP receptors coupled to a CAN channel in presympathetic neurons. Finally, we demonstrate this crosstalk modality to be critical for an optimal homeostatic sympathetic response to a central osmotic challenge (Bourque, 2008; Toney and Stocker, 2010).

Dendritically Released VP Mediates a Neurosecretory-to-Presympathetic Neuronal Crosstalk

We found that selective activation of a single neurosecretory VP neuron (either by photolytic NMDA uncaging or direct current injection in dual-patch recordings) evoked a V1a receptor-mediated depolarization and firing discharge in neighboring presympathetic (PVN-RVLM) neurons. Several lines of evidence support that the underlying mechanism involved activation of a CAN channel (Petersen, 2002), including (1) VP induced in PVN-RVLM neurons an increase in $[Ca^{2+}]_I$ that preceded the enhanced membrane excitability; (2) intracellular Ca^{2+} dependency of the VP effect; (3) voltage-dependent properties of I_{VP}, including an outwardly rectifying I/V curve; and (4) the I_{VP} reversal potential, characteristic of a mixed-cationic conductance. Although our pharmacological (FFA), immunohistochemical, and single-cell RT-PCR experiments (Figure S2) suggest the involvement of TRPM4 channels, recently reported to be present in MNNs (Teruyama et al., 2011), future studies are needed to identify the precise molecular identity of the underlying CAN channel.

Following bursts of action potentials, VP neurons express two types of opposing postspike membrane potentials: AHPs and DAPs. These potentials temporally overlap, competing

with each other to either inhibit or increase postfiring membrane excitability, respectively (Armstrong et al., 2010). We found that when prominent AHPs were observed in the stimulated VP neurons, the response latency of the presympathetic neurons was prolonged. This suggests that AHPs act as a "braking" system that efficiently regulate activity-dependent dendritic VP release and, consequently, the timing of the interneuronal crosstalk in the PVN.

MNNs project almost exclusively to the posterior pituitary (Swanson and Kuypers, 1980), with only a few reported cases of scarce axon collaterals, arising from but terminating outside the PVN (Hatton et al., 1985). Thus, the topographical segregation between the dendritic and axonal terminal fields of MNNs minimized the possibility that photolytically evoked VP released within the PVN originated from an axon terminal, rather than a dendritic source. This is further supported by our results showing that the evoked neurosecretory-presympathetic crosstalk persisted in the presence of TTX, which prevents axonal but not somatodendritic release of neuropeptides from MNNs. Similar to dorsal raphe serotonin neurons (de Kock et al., 2006), NMDA was shown to evoke dendritic release from MNNs in the absence of action potentials (de Kock et al., 2004), and dendritic VP release involves a Ca^{2+}-dependent exocytotic event (Ludwig et al., 2002). Accordingly, we found that photolysis of caged NMDA in the somata of VP neurons resulted in a rise in $[Ca^{2+}]_i$ both in neuronal somata and dendrites. This in turn was followed by an excitatory response in presympathetic neurons, which was prevented by a synaptic block media. Finally, intracellular Ca^{2+} chelation in VP neurons prevented the neurosecretory-presympathetic coupling observed in dual-patch recordings.

Although the combined anatomical, imaging, and electrophysiological data reported here strongly support a direct communication between neurosecretory and presympathetic neurons, we cannot conclusively rule out the participation of other intermediaries. For example, the evoked VP release from a single MNN could act in a recurrent positive feedback manner to recruit additional VP neurons to release further amounts of VP (Kombian et al., 1997; Ludwig and Leng, 1997). Moreover, dendritically released VP could also act on nearby astrocytes to evoke release of a potential gliotransmitter. However, our data showing that stimulation of VP neurons failed to consistently activate nearby astrocytes, and the fact that the neurosecretory-presympathetic coupling persisted following ablation of astrocyte function, would argue against this possibility.

Dendritically Released VP Acts as a Diffusible Interpopulation Signal Contributing to Homeostatic Neurohumoral Responses

Given its long half-life (~20 min in the brain; Mens et al., 1983), VP is ideally suited to act as a diffusible signal, potentially affecting multiple neurons at relatively distant locations. We found the firing activity of presympathetic PVN neurons to be tonically stimulated by an endogenous VP "tone," whose strength was enhanced either by increasing the activity of VP neurons or by prolonging VP lifetime in the ECS (aminopeptidase block) (Chen and Pittman, 1999). Conversely, the strength of the VP tone was diminished when VP neuronal activity was inhibited (κ opioid agonist) (Brown et al., 1998) or when the coefficient of diffusion of molecules in the ECS was lessened (5% dextran) (Piet et al., 2004). Thus, our findings support the ability of dendritically released VP from the neurosecretory population to act in a diffusible manner to modulate the activity of neighboring presympathetic neurons.

A central hyperosmotic challenge triggers a coordinated systemic release of VP, along with an increased RSNA (Bourque, 2008; Toney and Stocker, 2010). These responses are largely mediated by activation of neurosecretory and presympathetic SON/PVN neuronal populations, respectively (Antunes et al., 2006; Chen and Toney, 2001; Leng et al., 2001; Oliet and Bourque, 1993). In addition to systemic release, osmotic stimuli also evoke local

dendritic release of VP (Leng and Ludwig, 2008), which serves as a "population feedback" signal by which VP neurons autoregulate their own activity to optimize hormone secretion from their axonal terminals (Gouzènes et al., 1998). In this study, we found that a hyperosmotic-induced increase in RSNA was largely attenuated when V1a receptors within the PVN were locally blocked.

Given that VP MNNs are intrinsically osmosensitive (Oliet and Bourque, 1993), it is reasonable to speculate that osmotically driven dendritic VP release effectively augmented the endogenous neurosecretory VP tone, directly stimulating in turn the neighboring presympathetic neuronal population. Alternatively, dendritically released VP could also act by increasing presympathetic neuronal responsiveness to forebrain glutamatergic afferent inputs, known to contribute to osmotically driven sympathetic responses by the PVN (Antunes et al., 2006; Shi et al., 2007). This could occur either by strengthening osmosensitive glutamatergic afferents (i.e., pre- or postsynaptically) or simply by depolarizing the presympathetic resting membrane potential closer to spike threshold. We found that VP excitatory effects on presympathetic PVN neurons persisted in the presence of ionotropic glutamate receptor blockade, suggesting that a direct VP excitatory signal per se is sufficiently strong to evoke firing discharge and increase sympathetic outflow from the presympathetic neuronal population.

The extent to which other PVN neuronal populations are also targeted by dendritically released VP is at present unknown. Clearly, recruitment specificity is a critical factor for the generation of a physiologically relevant homeostatic response, which is likely achieved by the selective expression of V1a receptors in the relevant neuronal populations.

Collectively, our findings provide, to the best of our knowledge, the first demonstration that activity-dependent dendritic release of peptides constitutes an efficient interpopulation signaling modality in the brain. More specifically, they support our hypothesis that a local crosstalk between hypothalamic neurosecretory and presympathetic neuronal populations plays an important role in the generation of central integrative homeostatic responses (Pittman et al., 1982). Finally, given that neurohumoral activation (a process involving elevated neurosecretory and sympathetic outflows) is a hallmark in prevalent diseases such as hypertension and heart failure (Cohn et al., 1984; Esler et al., 1995; Pliquett et al., 2004), our studies provide insights into potentially pathophysiological mechanisms contributing to morbidity and mortality in these prevalent diseases.

EXPERIMENTAL PROCEDURES

Animals

Male Wistar rats (160–220 g) and male heterozygous transgenic VP-EGFP Wistar rats (5–6 weeks old) were used (Ueta et al., 2005). All procedures were carried out in agreement with the Georgia Regents University and the University of Nebraska Medical Center Institutional Animal Care and Use Committee guidelines, and were approved by the respective committees.

Retrograde Tracing

A total of 500 nl of rhodamine-labeled microspheres (Lumaflor) or cholera toxin B (CTB) (1%; List Biological Laboratories) was microinjected into the RVLM (starting from bregma: 12 mm caudal along the lamina, 2 mm medial lateral, and 8 mm ventral). The location of the tracer was verified histologically by Sonner et al. (2011). Animals were used 3–4 days after surgery.

Slice Preparation

Rats were anesthetized with pentobarbital (50 mg kg^{-1}), brains dissected out, and coronal slices (200 μm) of the hypothalamus containing the PVN were cut in an oxygenated ice-cold ACSF, as described by Sonner et al. (2011). For synaptic blockade, a 0.2 mM $CaCl_2$ and 400 μM $CdCl_2$ ACSF was used. In other cases, a 0 mM $CaCl_2$/3 mM EGTA solution was used, as indicated.

Electrophysiology

Hypothalamic slices were transferred to a recording chamber and superfused with ACSF (30°C–32°C) at a flow rate of ~3.0 ml min^{-1}. Conventional whole-cell patch-clamp recordings, using a K^+-gluconate-based internal solution, were obtained as previously described by Sonner et al. (2011). When noted, neurons were intracellularly labeled with Alexa Fluor 555 (100 μM) or biocytin (1%). Recordings were obtained from fluorescently labeled PVN-RVLM neurons and from EGFP-VP neurons. For bath-applied drugs, mean firing activity and membrane potential values were calculated from a 2 min period before drug application and in a 2 min period around the peak effect. For briefer applications (picospritzer) and uncaging, values were calculated from a 1 min period before and 10–20 s period around the peak effect, using Clampfit (Axon Instruments) or miniAnalysis (Synaptosoft) software.

Confocal Calcium Imaging

Neurons were loaded through the patch pipette with Fluo-5F pentapotassium salt (100 μM; Molecular Probes), as previously described (Filosa et al., 2006; Sonner et al., 2011). For astrocyte Ca^{2+} measurements, slices were incubated in ACSF containing Rhod2-AM and pluronic acid (2.5 μg/ml). Imaging was conducted using the Andor Technology Revolution system (iXON EMCCD camera with the Yokogawa CSU 10, confocal scanning unit). Fluorescence images were acquired at 488 nm and emitted light at >495 nm (Fluo5) or 561 nm and emitted light >607 nm (Rhod2). Images were acquired at a rate of 4 Hz. The fractional fluorescence (F/F_0) was determined by dividing the fluorescence intensity (F) within a region of interest (≈4.8 × 4.8 μm) by a baseline fluorescence value (F0) determined from 30 images before photolysis of caged NMDA. Data were analyzed using Andor IQ software (Andor Technology).

Photolysis of Caged Compounds

Slices were perfused with MNI-caged NMDA (50 μM). A UV laser excitation (405 nm) was directed to a region of interest drawn on the image of identified PVN-RVLM or EGFP-VP somata. Based on the pixel dwell time (200–800 μs) and the ROI area scanned (~40 μm^2), the uncaging protocol lasted 180–720 ms. For these experiments, an ACSF containing 20 μM Mg^{2+} was used to facilitate detection of evoked NMDA responses.

PVN Microinjections and In Vivo RSNA Measurements

Rats were anesthetized with urethane (0.75 g/kg i.p.) and α-chloralose (70 mg/kg i.p.) and placed in a stereotaxic apparatus. The coordinates for PVN micro-injections were 1.5 mm posterior to the bregma, 0.4 mm lateral to the midline, and 7.8 mm ventral to the dura. To record RSNA, the left kidney was exposed through a retroperitoneal flank incision. A branch of the renal nerve was isolated and placed on a pair of thin bipolar platinum electrodes. The electrical signal was amplified (10,000 times) with a Grass amplifier (P55) with a high-and low-frequency cutoff of 1,000 and 100 Hz, respectively. The peak response of RSNA to the administration of drugs into the PVN during the experiment (averaged over a period of 20–30 s) was expressed as a percent change from baseline (Biancardi et al., 2011).

Central Hyperosmotic Stimulation and VP Microdialysis

Injections of graded concentrations of NaCl (0.3, 0.9, and 2.1 Osm/l) were delivered through an internal carotid artery (ICA) catheter in a volume of 300 ml over a period of 10–15 s. For microdialysis, microdialysis probes were stereotaxically implanted with the U-shaped tip located within or adjacent to the right SON, as previously described (Ludwig et al., 2002): 1.0 mm posterior to bregma, 1.7 mm lateral to midline, 9.3 mm below the surface of the skull. After an equilibration period of at least 1 hr, consecutive 30 min dialysis samples were collected at a flow rate of 3 μl/min. After two 30 min baseline periods, rats were stimulated osmotically as described above, and a further two consecutive dialysate samples were collected, frozen, and stored at −20°C until assay for VP. The VP content in the microdialysates was measured by a highly sensitive and selective radioimmunoassay (Landgraf et al., 1995).

Immunohistochemistry

Rats were anesthetized with pentobarbital (50 mg kg^{-1}) and perfused transcardially in 4% paraformaldehyde in 0.01 M PBS. Brains were then removed, and coronal slices (30 μm) containing the PVN were cut and incubated with one or a combination of the following primary antibodies: rabbit (1:100; Millipore) or goat (1:50; Santa Cruz Biotechnology) anti-V1a receptor; goat anti-CTB (1:2500; List Biological Laboratories); rabbit anti-TRPM4 (1:2,000; kindly donated by Dr. Teruyama, LHSU); rabbit anti-MAP2 (1:500; Sigma-Aldrich); and mouse anti-DBH (1:20,000; Millipore). Incubation in primary antibodies was followed by specific fluorescently labeled secondary antibodies (1:250; Jackson ImmunoResearch Laboratories) for 4 hr. Slices were then rinsed and visualized using confocal microscopy (Carl Zeiss MicroImaging; 63× oil immersion, zoomed ×2; single optical plane = 0.5 μm thick) (Biancardi et al., 2010).

Single-Cell RT-PCR

Single-cell RT-PCR was carried out as previously described with minor modification (Sonner et al., 2011). The cytoplasm of the patched neuron, taking care not to contain the nucleus, was pulled into a patch pipette containing 2 μl DEPC-treated water and then mixed with 1 μl of RNase inhibitor (Applied Biosystems). A nested approach was used to quantify V1a receptor mRNA. The primers used included first-nested PCR (5′-CGAGGTGAACAATGGCACTAAAAC-3′ and 5′-TGTGATGGAAGGGTTTTCTGAATC-3′), second-nested PCR (5′-TCATCTGCTACCACATCTGGCG-3′ and 5′-GTGTAACCAAAAGCCCCTTATGAAAG-3′), primers for TRPM4 (5′-CCTGCAGGCCCAGGTAGAGA-3′ and 5′-TTCAGCAGAGCGTCCATGAG-3′), and GAPDH primers (5′-TTCAACGGCACAGTCAAGG-3′ and 5′-TGGTTCACACCCATCACAAA-3′). All primers were synthesized by Integrated DNA Technologies. Final PCR products were electrophoresed on a 2% agarose gel in TAE buffer (40 mM Tris-acetate, 1 mM EDTA [pH 8]) containing 0.5 μg/ml ethidium bromide, observed UV light, and photographed.

Statistical Analysis

All values are expressed as mean ± SEM. In most cases, unpaired or paired t tests were used, as indicated. One- or two-way ANOVA tests with Bonferroni post hoc tests were used as needed. Pearson's correlation test was used to determine if correlations existed between two parameters. Differences were considered significant at $p < 0.05$. All statistical analyses were conducted using GraphPad Prism (GraphPad Software).

Drugs

All drugs with the exception of MNI-caged NMDA (Tocris) were purchased from Sigma-Aldrich. For simplicity, the selective V1a antagonist β-mercapto-β,β-cyclopentamethylenepropionyl[1], [O-me-Tyr[2], Arg[8]]-VP (Sigma-Aldrich; V2255) is referred to as "V1a antagonist" throughout the manuscript.

Supplementary Material

Refer to Web version on PubMed Central for supplementary material.

Acknowledgments

We would like to thank Professor Rainer Landgraf for analyzing the microdialysis samples, Dr. Ryoichi Teruyama for the kind donation of the TRPM4 antibody, and Professor Gareth Leng for critical reading of the manuscript. This work was supported by NIH R01-HL090948-01 (to J.E.S.) and BBSRC BB/J004723/1 (to M.L.).

REFERENCES

Antunes VR, Yao ST, Pickering AE, Murphy D, Paton JF. A spinal vasopressinergic mechanism mediates hyperosmolality-induced sympathoexcitation. J. Physiol. 2006; 576:569–583. [PubMed: 16873404]

Armstrong WE, Wang L, Li C, Teruyama R. Performance, properties and plasticity of identified oxytocin and vasopressin neurones in vitro. J. Neuroendocrinol. 2010; 22:330–342. [PubMed: 20210845]

Biancardi VC, Campos RR, Stern JE. Altered balance of gamma-aminobutyric acidergic and glutamatergic afferent inputs in rostral ventrolateral medulla-projecting neurons in the paraventricular nucleus of the hypothalamus of renovascular hypertensive rats. J. Comp. Neurol. 2010; 518:567–585. [PubMed: 20034060]

Biancardi VC, Son SJ, Sonner PM, Zheng H, Patel KP, Stern JE. Contribution of central nervous system endothelial nitric oxide synthase to neurohumoral activation in heart failure rats. Hypertension. 2011; 58:454–463. [PubMed: 21825233]

Bourque CW. Central mechanisms of osmosensation and systemic osmoregulation. Nat. Rev. Neurosci. 2008; 9:519–531. [PubMed: 18509340]

Brown CH, Ludwig M, Leng G. kappa-opioid regulation of neuronal activity in the rat supraoptic nucleus in vivo. J. Neurosci. 1998; 18:9480–9488. [PubMed: 9801385]

Buijs RM, Van Eden CG. The integration of stress by the hypothalamus, amygdala and prefrontal cortex: balance between the autonomic nervous system and the neuroendocrine system. Prog. Brain Res. 2000; 126:117–132. [PubMed: 11105644]

Chen X, Pittman QJ. Vasopressin and amastatin induce V(1)-receptor-mediated suppression of excitatory transmission in the rat para-brachial nucleus. J. Neurophysiol. 1999; 82:1689–1696. [PubMed: 10515959]

Chen QH, Toney GM. AT(1)-receptor blockade in the hypothalamic PVN reduces central hyperosmolality-induced renal sympathoexcitation. Am. J. Physiol. Regul. Integr. Comp. Physiol. 2001; 281:R1844–R1853. [PubMed: 11705769]

Cheramy A, Leviel V, Glowinski J. Dendritic release of dopamine in the substantia nigra. Nature. 1981; 289:537–542. [PubMed: 6258083]

Cohn JN, Levine TB, Olivari MT, Garberg V, Lura D, Francis GS, Simon AB, Rector T. Plasma norepinephrine as a guide to prognosis in patients with chronic congestive heart failure. N. Engl. J. Med. 1984; 311:819–823. [PubMed: 6382011]

de Kock CP, Burnashev N, Lodder JC, Mansvelder HD, Brussaard AB. NMDA receptors induce somatodendritic secretion in hypothalamic neurones of lactating female rats. J. Physiol. 2004; 561:53–64. [PubMed: 15459239]

de Kock CP, Cornelisse LN, Burnashev N, Lodder JC, Timmerman AJ, Couey JJ, Mansvelder HD, Brussaard AB. NMDA receptors trigger neurosecretion of 5-HT within dorsal raphe nucleus of the rat in the absence of action potential firing. J. Physiol. 2006; 577:891–905. [PubMed: 17053037]

Ely DL. Organization of cardiovascular and neurohumoral responses to stress. Implications for health and disease. Ann. N Y Acad. Sci. 1995; 771:594–608. [PubMed: 8597433]

Esler MD, Lambert GW, Ferrier C, Kaye DM, Wallin BG, Kalff V, Kelly MJ, Jennings GL. Central nervous system noradrenergic control of sympathetic outflow in normotensive and hypertensive humans. Clin. Exp. Hypertens. 1995; 17:409–423. [PubMed: 7735286]

Filosa JA, Bonev AD, Straub SV, Meredith AL, Wilkerson MK, Aldrich RW, Nelson MT. Local potassium signaling couples neuronal activity to vasodilation in the brain. Nat. Neurosci. 2006; 9:1397–1403. [PubMed: 17013381]

Fuxe K, Dahlström A, Höistad M, Marcellino D, Jansson A, Rivera A, Diaz-Cabiale Z, Jacobsen K, Tinner-Staines B, Hagman B, et al. From the Golgi-Cajal mapping to the transmitter-based characterization of the neuronal networks leading to two modes of brain communication: wiring and volume transmission. Brain Res. Brain Res. Rev. 2007; 55:17–54.

Galarreta M, Hestrin S. Spike transmission and synchrony detection in networks of GABAergic interneurons. Science. 2001; 292:2295–2299. [PubMed: 11423653]

Ghamari-Langroudi M, Bourque CW. Flufenamic acid blocks depolarizing afterpotentials and phasic firing in rat supraoptic neurones. J. Physiol. 2002; 545:537–542. [PubMed: 12456832]

Gouzènes L, Desarménien MG, Hussy N, Richard P, Moos FC. Vasopressin regularizes the phasic firing pattern of rat hypothalamic magnocellular vasopressin neurons. J. Neurosci. 1998; 18:1879–1885. [PubMed: 9465012]

Guan JL, Kageyama H, Wang QP, Takenoya F, Kita T, Matsumoto H, Ohtaki T, Shioda S. Electron microscopy examination of galanin-like peptide (GALP)-containing neurons in the rat hypothalamus. Regul. Pept. 2005; 126:73–78. [PubMed: 15620417]

Hatton GI, Cobbett P, Salm AK. Extranuclear axon collaterals of paraventricular neurons in the rat hypothalamus: intracellular staining, immunocytochemistry and electrophysiology. Brain Res. Bull. 1985; 14:123–132. [PubMed: 2986791]

Kombian SB, Mouginot D, Pittman QJ. Dendritically released peptides act as retrograde modulators of afferent excitation in the supraoptic nucleus in vitro. Neuron. 1997; 19:903–912. [PubMed: 9354336]

Landgraf R, Neumann ID. Vasopressin and oxytocin release within the brain: a dynamic concept of multiple and variable modes of neuropeptide communication. Front. Neuroendocrinol. 2004; 25:150–176. [PubMed: 15589267]

Landgraf R, Neumann I, Holsboer F, Pittman QJ. Interleukin-1 beta stimulates both central and peripheral release of vasopressin and oxytocin in the rat. Eur. J. Neurosci. 1995; 7:592–598. [PubMed: 7620610]

Leng G, Ludwig M. Neurotransmitters and peptides: whispered secrets and public announcements. J. Physiol. 2008; 586:5625–5632. [PubMed: 18845614]

Leng G, Brown CH, Bull PM, Brown D, Scullion S, Currie J, Blackburn-Munro RE, Feng J, Onaka T, Verbalis JG, et al. Responses of magnocellular neurons to osmotic stimulation involves coactivation of excitatory and inhibitory input: an experimental and theoretical analysis. J. Neurosci. 2001; 21:6967–6977. [PubMed: 11517284]

Ludwig M. Dendritic release of vasopressin and oxytocin. J. Neuroendocrinol. 1998; 10:881–895. [PubMed: 9870745]

Ludwig M, Leng G. Autoinhibition of supraoptic nucleus vasopressin neurons in vivo: a combined retrodialysis/electrophysiological study in rats. Eur. J. Neurosci. 1997; 9:2532–2540. [PubMed: 9517458]

Ludwig M, Leng G. Dendritic peptide release and peptide-dependent behaviours. Nat. Rev. Neurosci. 2006; 7:126–136. [PubMed: 16429122]

Ludwig M, Sabatier N, Bull PM, Landgraf R, Dayanithi G, Leng G. Intracellular calcium stores regulate activity-dependent neuropeptide release from dendrites. Nature. 2002; 418:85–89. [PubMed: 12097911]

McBean GJ. Inhibition of the glutamate transporter and glial enzymes in rat striatum by the gliotoxin, alpha aminoadipate. Br. J. Pharmacol. 1994; 113:536–540. [PubMed: 7834205]

Mens WB, Witter A, van Wimersma Greidanus TB. Penetration of neurohypophyseal hormones from plasma into cerebrospinal fluid (CSF): half-times of disappearance of these neuropeptides from CSF. Brain Res. 1983; 262:143–149. [PubMed: 6831225]

Min MY, Rusakov DA, Kullmann DM. Activation of AMPA, kainate, and metabotropic receptors at hippocampal mossy fiber synapses: role of glutamate diffusion. Neuron. 1998; 21:561–570. [PubMed: 9768842]

Oliet SH, Bourque CW. Mechanosensitive channels transduce osmosensitivity in supraoptic neurons. Nature. 1993; 364:341–343. [PubMed: 7687327]

Petersen OH. Cation channels: homing in on the elusive CAN channels. Curr. Biol. 2002; 12:R520–R522. [PubMed: 12176374]

Piet R, Vargová L, Syková E, Poulain DA, Oliet SH. Physiological contribution of the astrocytic environment of neurons to intersynaptic crosstalk. Proc. Natl. Acad. Sci. USA. 2004; 101:2151–2155. [PubMed: 14766975]

Pittman QJ, Veale WL, Lederis K. Central neurohypophyseal peptide pathways: interactions with endocrine and other autonomic functions. Peptides. 1982; 3:515–520. [PubMed: 7122279]

Pliquett RU, Fasshauer M, Blüher M, Paschke R. Neurohumoral stimulation in type-2-diabetes as an emerging disease concept. Cardiovasc. Diabetol. 2004; 3:4. [PubMed: 15028121]

Pow DV, Morris JF. Dendrites of hypothalamic magnocellular neurons release neurohypophysial peptides by exocytosis. Neuroscience. 1989; 32:435–439. [PubMed: 2586758]

Salio C, Lossi L, Ferrini F, Merighi A. Neuropeptides as synaptic transmitters. Cell Tissue Res. 2006; 326:583–598. [PubMed: 16847638]

Shi P, Stocker SD, Toney GM. Organum vasculosum laminae terminalis contributes to increased sympathetic nerve activity induced by central hyperosmolality. Am. J. Physiol. Regul. Integr. Comp. Physiol. 2007; 293:R2279–R2289. [PubMed: 17898124]

Sonner PM, Lee S, Ryu PD, Lee SY, Stern JE. Imbalanced K+ and Ca2+ subthreshold interactions contribute to increased hypothalamic presympathetic neuronal excitability in hypertensive rats. J. Physiol. 2011; 589:667–683. [PubMed: 21149460]

Swanson LW, Kuypers HG. The paraventricular nucleus of the hypothalamus: cytoarchitectonic subdivisions and organization of projections to the pituitary, dorsal vagal complex, and spinal cord as demonstrated by retrograde fluorescence double-labeling methods. J. Comp. Neurol. 1980; 194:555–570. [PubMed: 7451682]

Swanson LW, Sawchenko PE. Paraventricular nucleus: a site for the integration of neuroendocrine and autonomic mechanisms. Neuroendocrinology. 1980; 31:410–417. [PubMed: 6109264]

Swanson LW, Sawchenko PE, Wiegand SJ, Price JL. Separate neurons in the paraventricular nucleus project to the median eminence and to the medulla or spinal cord. Brain Res. 1980; 198:190–195. [PubMed: 7407584]

Teruyama R, Armstrong WE. Calcium-dependent fast depolarizing afterpotentials in vasopressin neurons in the rat supraoptic nucleus. J. Neurophysiol. 2007; 98:2612–2621. [PubMed: 17715195]

Teruyama R, Sakuraba M, Kurotaki H, Armstrong WE. Transient receptor potential channel m4 and m5 in magnocellular cells in rat supraoptic and paraventricular nuclei. J. Neuroendocrinol. 2011; 23:1204–1213. [PubMed: 21848647]

Tobin VA, Hashimoto H, Wacker DW, Takayanagi Y, Langnaese K, Caquineau C, Noack J, Landgraf R, Onaka T, Leng G, et al. An intrinsic vasopressin system in the olfactory bulb is involved in social recognition. Nature. 2010; 464:413–417. [PubMed: 20182426]

Toney GM, Stocker SD. Hyperosmotic activation of CNS sympathetic drive: implications for cardiovascular disease. J. Physiol. 2010; 588:3375–3384. [PubMed: 20603334]

Ueta Y, Fujihara H, Serino R, Dayanithi G, Ozawa H, Matsuda K.-i. Kawata M, Yamada J, Ueno S, Fukuda A, Murphy D. Transgenic expression of enhanced green fluorescent protein enables direct visualization for physiological studies of vasopressin neurons and isolated nerve terminals of the rat. Endocrinology. 2005; 146:406–413. [PubMed: 15375027]

Ullrich ND, Voets T, Prenen J, Vennekens R, Talavera K, Droogmans G, Nilius B. Comparison of functional properties of the Ca2+-activated cation channels TRPM4 and TRPM5 from mice. Cell Calcium. 2005; 37:267–278. [PubMed: 15670874]

Xu HL, Mao L, Ye S, Paisansathan C, Vetri F, Pelligrino DA. Astrocytes are a key conduit for upstream signaling of vasodilation during cerebral cortical neuronal activation in vivo. Am. J. Physiol. Heart Circ. Physiol. 2008; 294:H622–H632. [PubMed: 18055520]

Zingg HH. Vasopressin and oxytocin receptors. Baillieres Clin. Endocrinol. Metab. 1996; 10:75–96. [PubMed: 8734452]

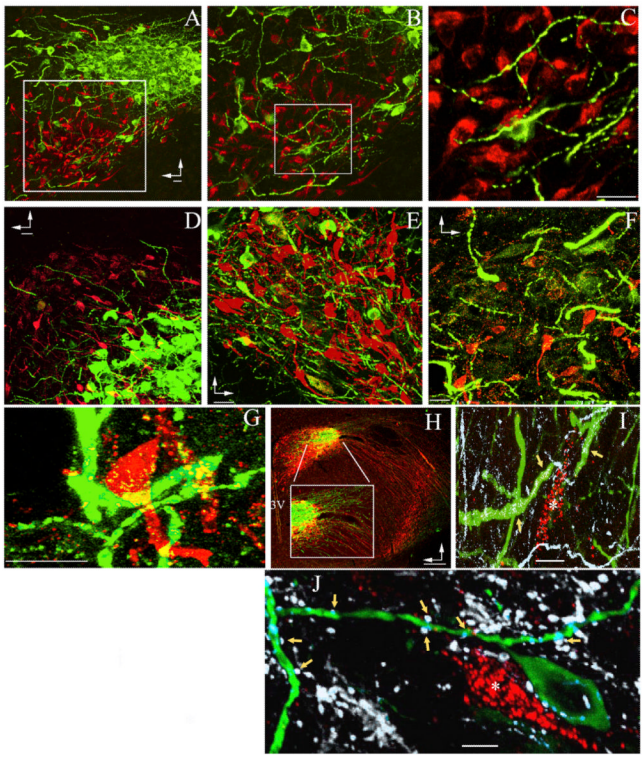

Figure 1. Dendro-Somatic and Dendro-Dendritic Interrelationships between Presympathetic and Magnocellular Neurosecretory PVN Neurons

(A–F) Confocal images showing the topographical segregation between immunoreactive magnocellular neurosecretory VP (green) and retrogradely labeled presympathetic PVN-RVLM (red) neuronal somata. In (A) and (B), the insets are shown at progressively higher magnification to better depict the presence of thick and varicose VP dendrites within the presympathetic neuronal compartment. Additional examples of VP dendrites extending from the lateral magnocellular subnucleus (C) into the three main presympathetic PVN subnuclei, including the dorsal cap (D), parvocellular ventromedial (E), and parvocellular posterior (F), are shown.

(G) PVN-RVLM neurons surrounded by VP dendrites are shown at high magnification.

(H) Low-magnification image of the PVN showing that the vast majority of immunoreactive VP (green) and OT (red) axons emerge from the PVN, running laterally and ventrally toward the median eminence. The box depicts a magnified view of the area between lines. 3V, third ventricle.

(I) Image showing thick, immunoreactive VP processes (green), which are also MAP2 immunoreactive (white, arrows), nearby a PVN-RVLM neuron (red, asterisk). Note the abundance of MAP2 processes that are negative for VP.

(J) Image showing DBH-immunoreactive boutons (white, arrows) abutting VP-immunoreactive processes (green) near a PVN-RVLM neuron (red, asterisk).

Vertical and horizontal arrows point dorsally and ventrally, respectively. Scale bars represent 20 μm in (A)–(G), 200 μm in (H), and 5 μm in (I) and (J).

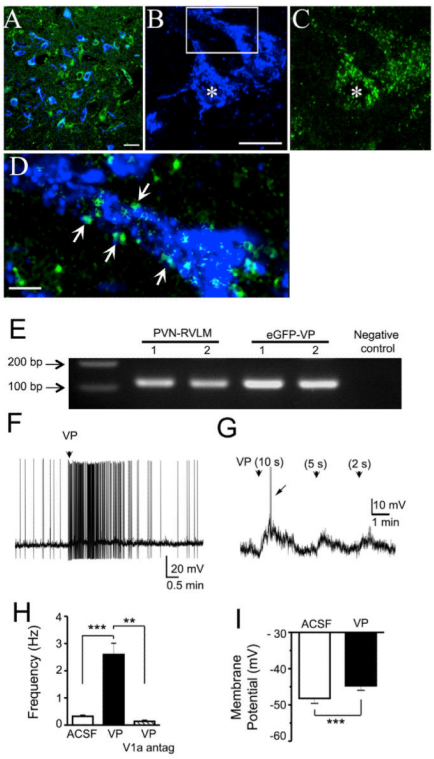

Figure 2. Presympathetic PVN Neurons Express Functional V1a Receptors

(A–D) Sample confocal images at low- (A) and high (B–D)-magnification showing CTB retrogradely labeled PVN-RVLM neurons (blue) and V1a receptor immunoreactivity (green; Millipore primary antibody) in the PVN. In (B) and (C), examples of two PVN-RVLM neurons showing dense V1a-immunoreactive clusters, respectively, are depicted. In (D), the squared area in (B) is shown at an expanded scale to better show V1a-immunoreactive clusters (arrows) located at the surface of the shown dendrite. Asterisks in (B) and (C) indicate the soma of the same sampled neuron.

(E) Single-cell V1a mRNA expression in identified PVN-RVLM and EGFP-VP neurons. A nontemplate negative control is shown in the right lane, and a small piece of a DNA ladder is shown in the left lane.

(F) A puff of VP (1 μM, arrowheads) delivered directly onto a presympathetic PVN-RVLM neuron evokes a high-frequency burst of action potentials.

(G) Sample trace showing that in the presence of TTX (0.5 μM), puffs of VP of decremental durations depolarized a presympathetic PVN neuron in a proportionally decremental manner. Note the presence of Ca^{2+} spikes (arrow).

(H and I) Summary data of VP effects on firing activity (H) and membrane potential (I) in presympathetic neurons (n = 16). Error bars represent SEM. **p < 0.01 and ***p < 0.001. antag., antagonist.

Scale bars represent 20 μm in (A) and (B) and 2.5 μm in (D). See also Figure. S1.

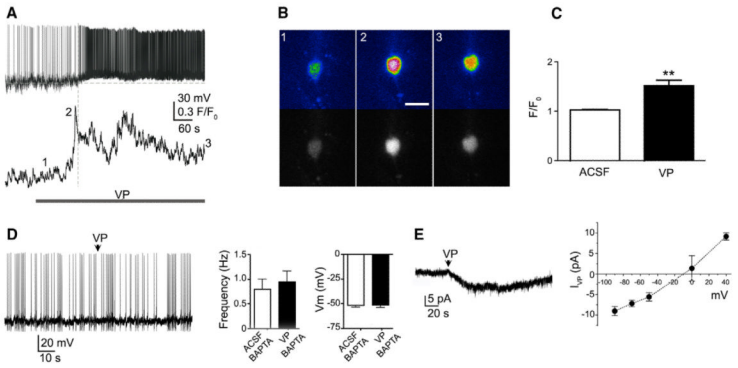

Figure 3. VP Effects on Presympathetic Neurons Involve an Increase in $[Ca^{2+}]_I$ and Activation of a CAN Channel

(A) Sample traces showing simultaneous $\Delta[Ca^{2+}]_I$ (lower) and membrane potential (upper) measurements in a PVN-RVLM neuron in response to bath-applied VP (1 μM, line). Note that the increase in $\Delta[Ca^{2+}]_I$ preceded the increase in firing discharge.

(B) Representative pseudocolor (upper) and black and white (lower) images of VP-evoked Ca^{2+} changes in the PVN-RVLM neuron shown in (A). Image numbers correspond to the time points shown in (A).

(C) Summary data showing mean VP-evoked Ca^{2+} changes (F/F_0) in presympathetic PVN neurons (n = 8). **p < 0.01.

(D) Sample trace and summary data showing that chelation of intracellular Ca^{2+} with BAPTA (10 mM) in the patch pipette prevented VP excitatory effect (puff, arrowhead) in presympathetic PVN neurons (n = 8).

(E) Sample trace in voltage-clamp mode showing a VP-mediated (puff, arrowhead) inward current (I_{VP}) in a presympathetic PVN neuron. The right panel shows a mean I/V plot of I_{VP} evoked at various holding potentials (n = 5).

Error bars represent SEM. See also Figure S2.

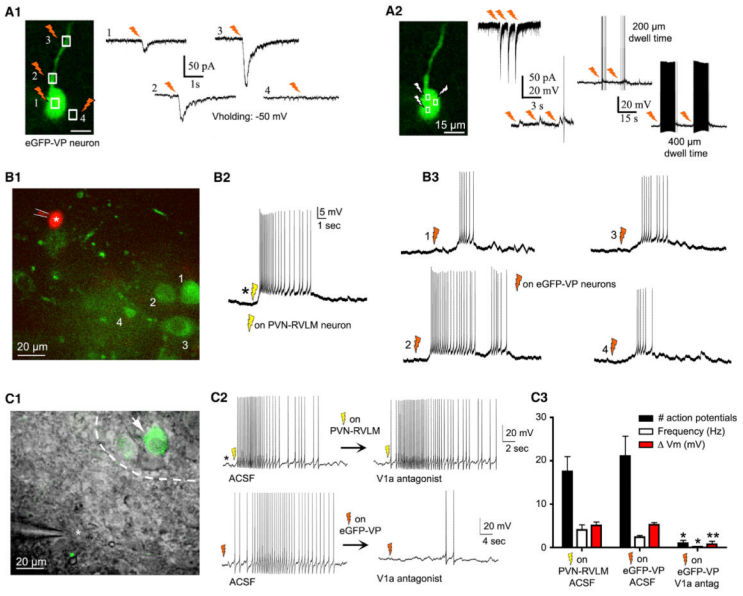

Figure 4. Photoactivation of Neurosecretory VP Neurons Evokes a V1a Receptor-Mediated Excitatory Response in Neighboring Presympathetic Neurons

(A) Inward currents evoked in a patched EGFP-VP neuron following photolysis of caged NMDA onto various somatodendritic regions of interest (ROI) (1–3). Note that photolysis in an ROI a few microns away from the recorded neuron (4) failed to evoke a response. (A2) Repetitive laser photolysis of caged NMDA onto the same EGFP-VP neuron evoked reproducible inward currents (upper trace), membrane depolarizations (lower trace), and bursts of action potentials (right traces).

(B) Slice containing a patched presympathetic PVN-RVLM neuron (red, asterisk) and neighboring EGFP-VP neurons (green, 1–4) that were activated with photolysis of caged NMDA. (B2) Direct uncaging of NMDA onto the patched presympathetic neuron (asterisk, yellow flashes) evoked a burst of action potentials. (B3) Burst of action potentials recorded in the patched presympathetic neuron in response to uncaging of NMDA onto the EGFP-VP neurons shown in (B1) (1–4, red flashes). Note the delayed response in the PVN-RVLM neurons compared to (B2).

(C) Combined DIC and fluorescence image of a slice containing a patched presympathetic neuron (asterisk) and neighboring EGFP-VP neurons (green). Arrow points to the stimulated EGFP-VP neuron. The dashed line delimits the ventral border of the lateral magnocellular subnucleus. (C2) Presympathetic neuronal responses to uncaging of NMDA onto the recorded PVN-RVLM neuron (upper traces) or onto an EGFP-VP neuron (arrow in C1, and lower traces) in control ACSF (left) and in the presence of a V1a receptor antagonist (right). (C3) Summary data of mean changes in the number of action potentials, action potential frequency, and membrane potential in presympathetic PVN-RVLM neurons, evoked by photolysis of caged NMDA onto the presympathetic neurons themselves (n = 11, left) or onto EGFP-VP neurons in the absence (n = 38, middle) or presence (n = 7, right) of the V1a antagonist. Error bars represent SEM. *$p < 0.01$ and **$p < 0.001$ versus respective ACSF. See also Figures S3, S4, S5, and S6.

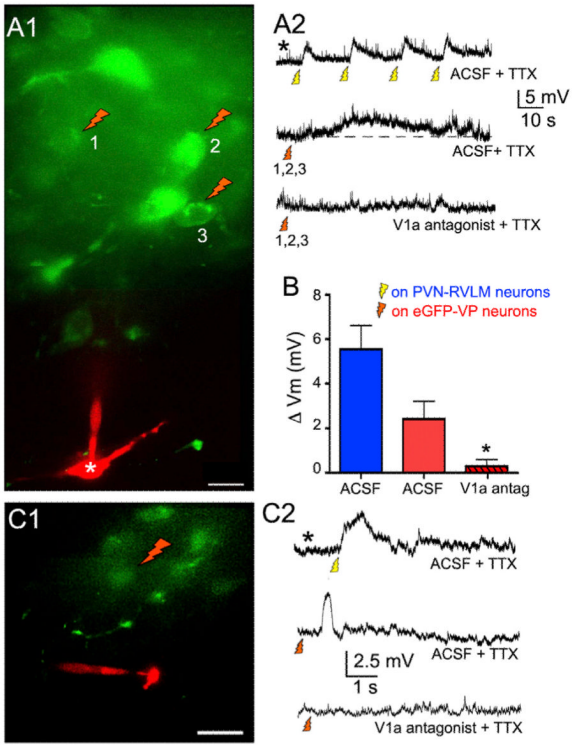

Figure 5. The NMDA-Mediated Crosstalk between Neurosecretory VP and Presympathetic PVN-RVLM Neurons Is Not Dependent on Action Potential Firing

(A) Sample of a slice containing a patched presympathetic PVN-RVLM neuron that was loaded with Alexa Fluor 555 (red, asterisk) and neighboring EGFP-VP neurons (green) that were photoactivated with caged NMDA. “1,” “2,” and “3” indicate three EGFP-VP neurons that were simultaneously activated by NMDA uncaging. (A2) Representative traces obtained from the recorded PVN-RVLM neuron following five repetitive photolysis of caged NMDA directly onto the recorded cell (upper trace, yellow flashes) or in response to simultaneous photolysis onto the three EGFP-VP neurons (1–3, red flashes) shown in (A1), in control ACSF + 1 μM TTX (middle trace), and following bath application of the V1a receptor antagonist + TTX (lower trace).

(B) Summary data of mean changes in PVN-RVLM membrane potential evoked in the presence of TTX following photolysis of caged NMDA onto the presympathetic neurons themselves (n = 6, blue bar) or onto EGFP-VP neurons (red bars) in the absence (n = 18, middle bar) or presence (n = 14, right bar) of the V1a receptor antagonist. Error bars represent SEM. *p < 0.01 versus respective ACSF.

(C) Another example showing a recorded presympathetic PVN-RVLM neuron (Alexa Fluor 555; red) and a photoactivated EGFP-VP neuron (green, arrow). (C2) Sample traces obtained from the PVN-RVLM neuron from (C1) following photolysis of caged NMDA in the presence of 1 μM TTX directly onto the PVN-RVLM neuron itself (asterisk, upper trace, yellow flash) or onto an EGFP-VP neuron (red flashes), in control ACSF (middle trace), and following bath application of the V1a receptor antagonist (lower trace),in the presence of TTX.

Scale bars represent 15 μm.

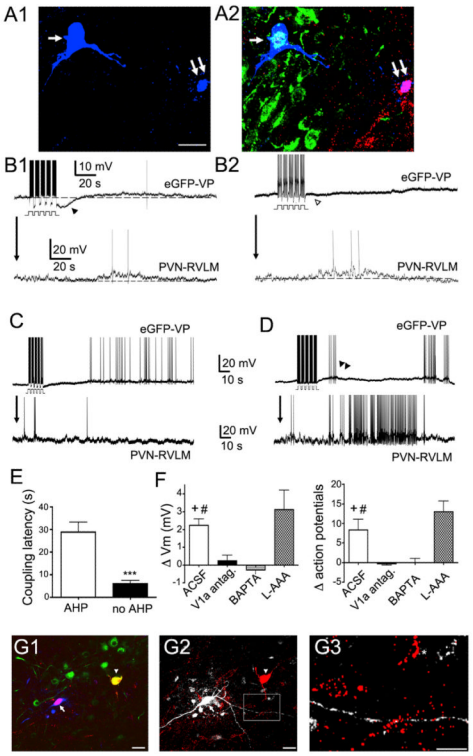

Figure 6. Neurosecretory-Presympathetic Crosstalk Unveiled during Dual-Patch Recordings from EGFP-VP and PVN-RVLM Neurons

(A) Sample pair of intracellularly labeled (Alexa 633; blue, arrows) PVN neurons during simultaneous dual-patch recordings. The identity of the patched neurons as EGFP-VP (cyan, single arrow) and retrogradely labeled PVN-RVLM (purple, double arrow) is shown in (A2).

(B) Electrically evoked bursting activity in the EGFP-VP neuron resulted in a delayed membrane depolarization and increased firing discharge in the neighboring PVN-RVLM neuron. Note the pronounced AHP following action potential firing in the EGFP-VP neuron (filled arrowhead). (B2) Another sample of paired recordings showing a similar response. Note, however, the lack of AHP in the EGFP-VP neuron (empty arrowhead) and the shorter latency of the evoked PVN-RVLM response.

(C) Sample of a paired recording in which the EGFP-VP neuron was dialyzed with BAPTA. Note the lack of response in the PVN-RVLM neuron.

(D) Sample of a paired recording in the presence of L-AAA (250 μM, 30 min), showing an increase in PVN-RVLM firing activity following stimulation of the EGFP-VP neuron. Note the presence of a DAP in the EGFP-VP neuron (double filled arrowheads) and the brief latency for the evoked PVN-RVLM response.

(E) Comparison of the mean interneuronal-coupling latency in EGFP-VP neurons displaying or not an AHP following the evoked burst of action potentials (n = 10 and 8, respectively).

(F) Summary data of mean changes in PVN-RVLM membrane potential (left) and firing activity (right) following direct stimulation of EGFP-VP neurons in control ACSF (n = 13), V1a antagonist (n = 7), intracellular BAPTA in the stimulated EGFP-VP neuron (n = 5), and in the presence of L-AAA (n = 5).

(G) Another representative example of dual-patched and intracellularly labeled EGFP and PVN-RVLM neurons. (G1) Single focal plane of a confocal image showing EGFP-VP (green) and PVN-RVLM (red) neurons. The recorded PVN-RVLM neuron was intracellularly filled with Alexa 633 (arrow; colocalization is indicated in purple), and the

recorded EGFP-VP neuron was intracellularly filled with Alexa Fluor 555 (arrowhead; colocalization is indicated in yellow). (G2) is the same image as in (A1), but a confocal stack of ten images is shown to better depict the dendritic processes of the recorded neurons. The blue color has been transformed to white for better clarity. Asterisk points to a dendritic end of the EGFP-VP (Alexa Fluor 555; filled) neuron. In (G3), the squared area in (G2) is shown at a magnified scale.

Error bars represent SEM. $^{**}p < 0.001$ versus AHP; $^{+}p < 0.05$ and $^{\#}p < 0.01$ versus V1a antagonist and BAPTA, respectively. Scale bars represent 25 μm in (A1), 20 μm in (G1) and (G2), and 10 μm in (G3). Action potentials were cropped.

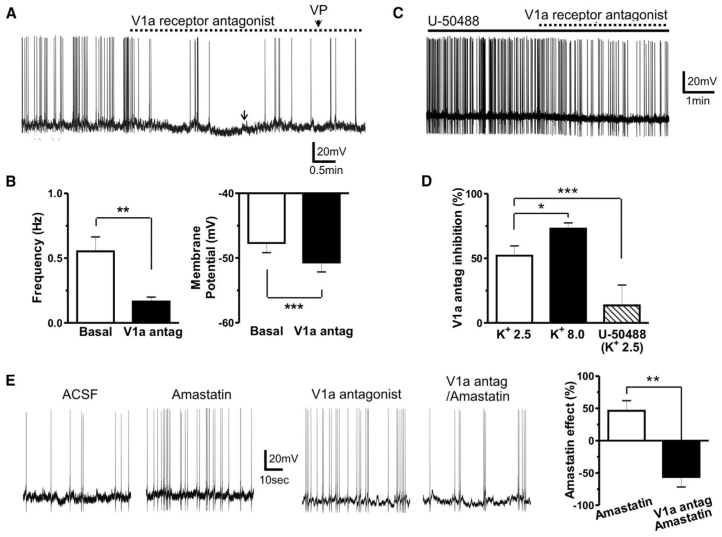

Figure 7. An Activity-Dependent Diffusible Pool of Dendritically Released VP Tonically Modulates Presympathetic Neuronal Activity

(A) Sample trace showing a hyperpolarization and diminished firing discharge of a presympathetic neuron following bath application of the V1a receptor blocker (1 μM). At the arrow, DC current injection was applied to bring the membrane potential back to control levels to show that the V1a antagonist efficiently blocked the neuronal response to a VP puff (1 μM, arrowhead).

(B) Summary data of the effects of the V1a receptor antagonist on firing frequency and membrane potential of presympathetic neurons (n = 14).

(C) Sample trace showing a blunted effect of the V1a receptor antagonist in the presence of the κ receptor agonist U-50488 (1 μM).

(D) Summary data of the effects of the V1a antagonist on presympathetic neuronal firing in control ACSF (K^+ 2.5 mM), high K^+ ACSF (8.0 mM), and in U-50488 (K^+ 2.5 mM) (n = 6, 7 and 8, respectively).

(E) Sample traces and summary data showing the effects of the aminopeptidase blocker amastatin (10 μM, 10 min) in control ACSF and in the presence of the V1a receptor antagonist (n = 8 in each group).

Error bars represent SEM. *p < 0.05, **p < 0.01, and ***p < 0.001. See also Figure S7.

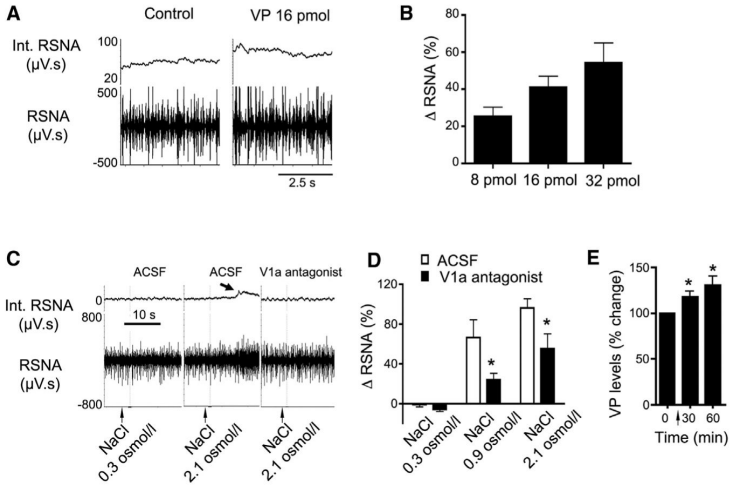

Figure 8. Dendritic Release of VP within the PVN Contributes to Sympathoexcitatory Homeostatic Responses following a Central Hyperosmotic Challenge

(A) Representative traces showing changes in raw (lower) and integrated (Int.; upper) RSNA following administration of VP (16 pmol) onto the PVN.

(B) Summary data showing dose-dependent increases in RSNA after microinjections of VP (8, 16, and 32 pmol) onto the PVN ($p < 0.02$, one-way ANOVA; $n = 9$).

(C) Representative traces showing changes in RSNA following intracarotid infusions of an isosmotic (NaCl 0.3 Osm/l) or hyperosmotic (NaCl 2.1 Osm/l) solution, following bilateral microinjections of ACSF or of the V1a receptor antagonist (2 nmol/100 nl, 6–10 min before the osmotic challenge) into the PVN. Note the increase in RSNA evoked by the hyperosmotic challenge in control ACSF (arrow), but not in the presence of the V1a receptor antagonist.

(D) Summary data showing dose-dependent increases in RSNA after intracarotid infusions of NaCl (0.3, 0.9, and 2.1 Osm/l) in animals that received an intra-PVN microinjection of either ACSF or the V1a receptor antagonist (*$p < 0.0001$ versus respective ACSF; $n = 7$).

(E) Summary data showing increased VP content in 30 min microdialysates sampled from the SON before and after an intracarotid infusion of NaCl 2.1 Osm/l (arrow) (*$p < 0.05$ versus basal levels; $n = 7$).

Error bars represent SEM.